Article:
Wang, A., Fei, M., Song, Y. et al. (2026) Scalable Voltage Control for DC Microgrids: Robustness to Network Structural Variations. IEEE Transactions on Smart Grid, 17 (1). pp. 603-616. ISSN: 1949-3053

https://doi.org/10.1109/tsg.2025.3614577

Scalable Voltage Control for DC Microgrids: Robustness to Network Structural Variations

Aimin Wang, *Graduate Student Member, IEEE,* Minrui Fei, Yang Song, *Member, IEEE*, Dajun Du, *Member, IEEE*, Chen Peng, *Senior Member, IEEE*, Kang Li, *Senior Member, IEEE*

***Abstract*—Frequent plug-in/-out operations result in structural variations of DC microgrids (DCmGs), posing challenges to scalable control and often requiring costly redesigns to maintain stability. To address this issue, this paper proposes a scalable voltage control strategy for uncertain DCmGs, enabling plug-and-play functionality without controller redesign or system reconfiguration. A polytopic uncertain DCmG model is first formulated to simultaneously capture parameter uncertainties in distributed generation units (DGUs), power lines, and ZIP (i.e., impedance, current, and power) loads. A structured free-weight matrix technique is then developed to mitigate the adverse effects of line and load uncertainties on DGUs while yielding a more tractable linear matrix inequality formulation. The proposed scalable control method is implemented locally to ensure the dissipative voltage stability of each DGU, thereby preserving the dissipativity of the entire network. Numerical simulations validate the effectiveness of the proposed strategy in achieving faster convergence and reduced overshoot.**

***Index Terms*—DC microgrids (DCmGs), plug-and-play, polytopic uncertainties, scalable control, ZIP loads.**

I. Introduction

THE growing concerns about energy crises and climate change, combined with the rapid advancement of renewable energy source (RES) technologies such as solar, wind, and fuel cells, have spurred the deployment of microgrids worldwide [1]–[3]. Microgrids are increasingly recognized as essential components of modern power systems, serving as flexible platforms for integrating diverse RESs [4]. Typically, these systems comprise multiple renewable distributed generation units (DGUs) that supply power to local loads and are interconnected via power lines [5]. Compared with AC microgrids [6], DC microgrids (DCmGs) eliminate the need for frequency and reactive power regulation, as well as harmonic compensation [7]. Recent advances in power electronics have further facilitated the utilization of DCmGs across various applications, including electric vehicles, avionics, and marine systems [8].

Despite these technological advantages, DCmGs are susceptible to voltage instability when subjected to complex load conditions, which typically include constant impedance load (CIL), constant current load (CCL), and constant power load (CPL) [9]–[11]. To tackle these challenges, numerous control strategies have been proposed, such as optimal voltage control for CILs [12], observer-based approaches for CCLs [13], and advanced nonlinear control methods for CPLs, including backstepping [14], H_∞ control [15], T-S fuzzy control [16], and sliding mode control [17]. For DCmG systems subject to uncertain CPLs, a polytopic robust control approach has been developed in [18], modeling CPL uncertainties using convex hull vertices. Nevertheless, most existing studies focus on CIL, CCL, or CPL individually, lacking a unified framework capable of simultaneously handling a comprehensive ZIP load model, which is a parallel combination of the aforementioned load types. Moreover, current robust control designs typically address uncertainties in either the load or the DGU components in isolation. To date, no comprehensive control strategy has been developed that robustly stabilizes DCmGs with simultaneous uncertainties in DGUs, power lines, and ZIP loads, thus revealing a critical gap in the literature.

Scalability is another essential requirement for practical DCmG control, referring to the ability to design local controllers independently of the global network size or topology. This feature is especially relevant in scenarios where DGUs are temporarily unplugged to improve energy efficiency and reduce operational costs during low-load conditions [19], or plugged out due to maintenance or faults [20]. Conversely, additional DGUs may be plugged in during peak load periods to enhance system support, such as when high-power equipment (e.g., heavy-duty industrial motors) is connected [21]. These plug-and-play (PnP) operations, however, lead to abrupt changes in both network structure and subsystem count. From an engineering standpoint, each plug-in or plug-out operation generally requires redesigning the control structure and reconfiguring the system topology, resulting in substantial engineering costs and operational complexity due to labor, downtime, and system recommissioning [22].

To address this issue, various scalable control strategies have been proposed to enable the seamless integration and disconnection of DGUs without compromising overall system stability. For instance, Riverso et al. [23] have introduced a scalable control method for AC microgrids based on a separable storage function (SSF) technique, which was later extended into decentralized scalable control [24] and neural network-based adaptive control [25] for DCmGs using linear matrix inequality (LMI) formulations. A passivity-based scalable control approach has been developed in [26] for DCmGs

This work was supported in part by the Natural Science Foundation of China (NSFC) under Grant U24A20259, Grant 62173217, and Grant 62203290; and in part by the 111 Project under Grant D18003. *(Corresponding author: Minrui Fei.)*

Aimin Wang, Minrui Fei, Yang Song, Dajun Du, and Chen Peng are with the Shanghai Key Laboratory of Power Station Automation Technology, School of Mechatronic Engineering and Automation, Shanghai University, Shanghai 200072, China (e-mail: amwang@shu.edu.cn; mrfei@staff.shu.edu.cn; y_song@shu.edu.cn; ddj@i.shu.edu.cn; c.peng@i.shu.edu.cn).

Kang Li is with the School of Electronics and Electrical Engineering, University of Leeds, Leeds LS2 9JT, U.K. (e-mail: k.li1@leeds.ac.uk).

TABLE I
COMPARATIVE ANALYSIS BETWEEN THE CONTRIBUTIONS OF THIS PAPER AND THE EXISTING RESULTS IN THE LITERATURE

Ref.[1]	TL[2]/UL[3]	RIL[4]	UL[5]/RIL[6]	Sca.[7]	ASSF[8]
[12]	CIL[9]/✗	✗	✗/✗	✗	–
[13]	CCL[10] /✗	✗	✗/✗	✗	–
[14]	CPL[11] /✗	✗	✗/✗	✗	–
[15]	CPL/✗	✗	✗/✗	✗	–
[16]	CPL/✗	✗	✗/✗	✗	–
[17]	CPL/✗	✗	✗/✗	✗	–
[18]	CPL/✔	✗	✗/✗	✗	–
[23]	CCL/✗	✗	✗/✔	✔	✗
[24]	CCL/✗	✗	✗/✔	✔	✗
[25]	CPL/✗	✗	✔/✔	✔	✗
[26]	ZIP/✗	✗	✗/✔	✔	✗
†[12]	ZIP/✔	✔	✔/✔	✔	✔

[1]References. [2]Types of loads. [3]Uncertain loads.
[4]Remove impacts of loads. [5]Uncertain lines.
[6]Remove impacts of lines. [7]Scalability.
[8]Avoid separable storage function.
[9]Constant impedance load. [10]Constant current load.
[11]Constant power load. [12]This paper.

with ZIP loads, assuming well-posed and skew-symmetric interconnections. Despite their contributions, existing scalable control methods face two critical limitations: they typically require neighboring DGUs to update their controllers in response to every plug-in or plug-out event, and their reliance on SSFs with block-diagonal matrix constraints often leads to LMI infeasibility when system uncertainties are present. Under such conditions, PnP operations may be constrained, and forced execution could jeopardize system stability or even lead to outages. To the best of the authors' knowledge, a significant gap still exists in the literature for a scalable control strategy that ensures robustness against uncertainties in DGUs, power lines, and ZIP loads, while preserving the original controller structure and ensuring the admissibility of all plug-in/-out requests.

Motivated by the aforementioned research gaps, the following challenges need to be addressed:

(1) How to formulate a unified DCmG model that captures multi-source uncertainties from ZIP loads, power lines, and DGUs?
(2) How to design a scalable controller without relying on restrictive SSF structures, thereby avoiding the rejection of PnP operations?
(3) What theoretical stability and performance guarantees can be provided for the proposed control scheme under dynamic operating conditions?

To cope with these challenges, this paper presents a scalable dissipative control scheme for voltage regulation in uncertain DCmGs by developing a structured free-weight matrix (SFWM) technique. Table I compares the proposed method with representative existing strategies. It can be clearly seen that the existing results have primarily focused on SSF-based scalable control methods, whereas the proposed new scalable scheme pays its attention to the SFWM technique with polytopic uncertainties. The main contributions of this study are summarized as follows:

(1) In contrast to [12]–[18], which address CIL, CCL, or CPL individually and overlook uncertainties stemming from DGUs, power lines, and ZIP loads, this paper proposes a unified uncertain DCmG architecture that simultaneously captures parametric uncertainties in DGUs, power lines, and ZIP loads. The uncertain DCmG dynamics are represented by a polytopic model, capturing parameter variations at the vertices of a convex hull.
(2) Unlike conventional SSF-based scalable control schemes [23]–[26], where the LMI optimization problem may become infeasible or overly conservative due to block-diagonal constraints on the Lyapunov matrix, this paper proposes a scalable voltage control strategy leveraging an SFWM technique. The SFWM relaxes the constraints induced by SSFs and eliminates cross-product terms between uncertain system matrices and storage functions. This results in a more tractable and less conservative LMI formulation, ensuring that all plug-in/-out requests for DGUs are always admissible.
(3) The proposed scalable control method is locally implemented based solely on DGU parameters and is independent of power lines, ZIP loads, or adjacent DGUs. Therefore, the plugging in or out of a DGU only leads to an augmentation or reduction of a local set of LMI conditions. During the PnP process, the method ensures dissipative stability while preserving the original control structure and avoiding network reconfiguration. Additionally, simulation results under varying conditions verify the proposed method's superior performance in terms of faster convergence speed and reduced voltage overshoot compared with existing approaches [24] and [25].

The structure of this paper is as follows. Section II develops a unified uncertain model for DCmGs, capturing parametric uncertainties in DGUs, power lines, and ZIP loads through a polytopic representation. Section III presents the decentralized dissipativity analysis and scalable controller design. Section IV demonstrates the effectiveness and superiority of the proposed control scheme through numerical simulations. Finally, Section V concludes the paper and discusses potential directions for future research.

Notations: The set of all real matrices of size $m \times n$ is denoted by $\mathbb{R}^{m\times n}$, with null matrices represented by $\mathbf{0}^{m\times n}$. The identity matrix of appropriate dimension is denoted by $\mathbf{I}$. The vector $\mathbf{1}_\ell \in \mathbb{R}^\ell$ denotes a column vector with all entries equal to 1. A matrix $W \in \mathbb{R}^{n\times n}$ is said to be negative definite (or positive definite) if $W < 0$ (or $W > 0$). The parameters $\overline{\varphi}$ and $\underline{\varphi}$ denote the maximum and minimum values of the variable φ, respectively. The symbol * denotes the symmetric part of a symmetric matrix. The operator diag$\{\cdot\}$ constructs a diagonal matrix by placing the elements of a vector along its main diagonal. The superscript $(\cdot)^T$ denotes the transpose of a matrix or vector.

II. SYSTEM MODELING OF DCMGS WITH ZIP LOADS

Graph Theory: The system information flow is modeled as an undirected graph $\mathcal{G} = (\mathcal{V}, \mathcal{E}, \mathcal{A})$, where $\mathcal{V} = \{1, 2, ..., n\}$ represents the set of nodes, $\mathcal{E} \subset \mathcal{V} \times \mathcal{V}$ denotes the edge set,

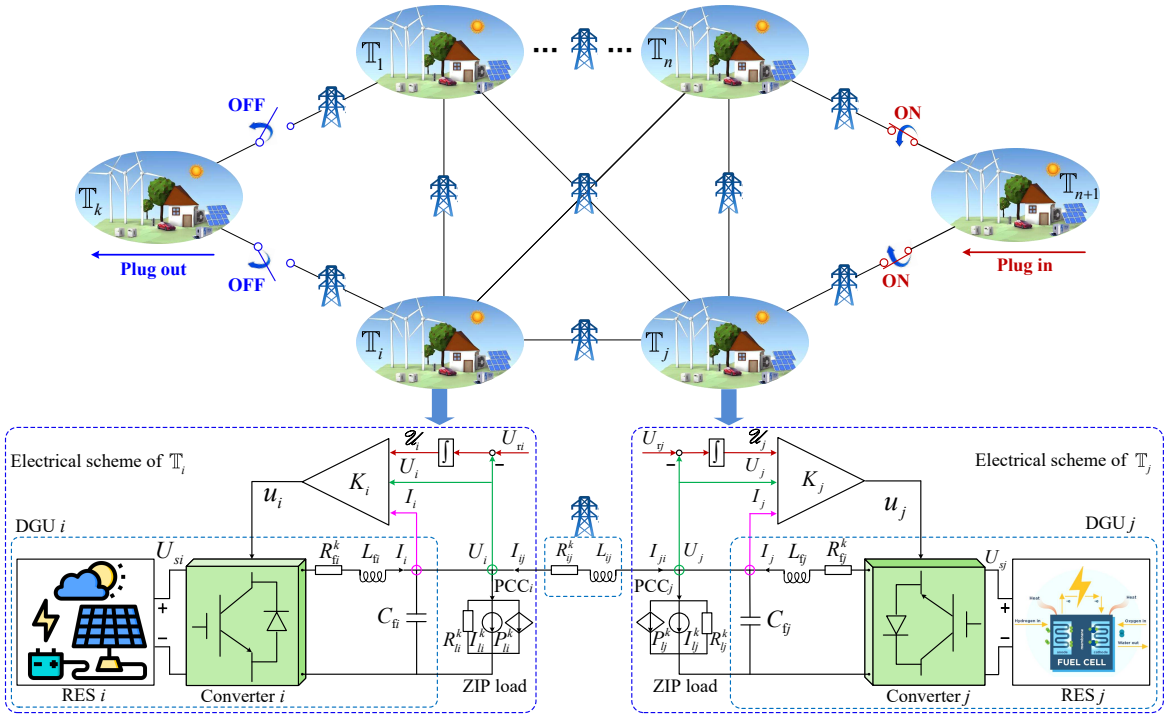

Fig. 1. Overall framework of the proposed scalable voltage control for uncertain DCmGs interconnected via power lines under dynamic plug-in/-out scenarios.

TABLE II
ELECTRICAL PARAMETERS OF A DCMG SUBSYSTEM

Parameters	Electrical meanings
U_i, U_{ri}	Voltage signal at the PCC i and its reference
I_i	Filter current in DGU i
$\mathscr{U}_i$	Local integrator state
u_i	Control signal to converter i
R_{ij}	Impedance of power lines
$R_{\mathrm{f}i}$, $L_{\mathrm{f}i}$, $C_{\mathrm{f}i}$	Impedance, inductance, and capacitance of the filter
R_{li}, I_{li}, P_{li}	Impedance, current, and power demand of ZIP loads

and $\mathcal{A} = [a_{ij}] \in \mathbb{R}^{n\times n}$ is the associated adjacency matrix. For each node $i \in \mathcal{V}$, the self-loop condition $a_{ii} = 0$ implies no self-information flow. A directed edge $(j, i) \in \mathcal{E}$ is assigned a weight a_{ij}, where $a_{ij} > 0$ if the edge exists, and $a_{ij} = 0$ otherwise. The neighborhood of node i is denoted by $\mathcal{N}_i$. The in-degree matrix $\mathcal{D}$ is a diagonal matrix with entries $d_i = \sum_{j\in\mathcal{N}_i} a_{ij}$. The Laplacian matrix is defined as $\mathcal{L} = \mathcal{D} - \mathcal{A}$.

A. Local Subsystem Model of DCmG

As illustrated in the lower dashed block of Fig. 1, each DCmG subsystem corresponds to a node in the graph and comprises a local controller, a ZIP load, and a DGU. Specifically, each DGU integrates a RES, a series RLC filter, and a power converter. The power converter functions as the interface between the DGU and its local controller, while simultaneously regulating the power delivered to the load at the point of common coupling (PCC). These subsystems are interconnected via power lines, which are interpreted as graph edges and serve as the sole medium for both power transfer and implicit communication. The power lines are modeled using the quasi-stationary line approximation [25].

By applying Kirchhoff's voltage and current laws to Fig. 1, the local subsystem dynamics can be derived as

$$\begin{cases} \dot{U}_i = \dfrac{1}{C_{\mathrm{f}i}} I_i + \displaystyle\sum_{j\in\mathcal{N}_i} \frac{1}{R_{ij}C_{\mathrm{f}i}}(U_j - U_i) - \frac{1}{C_{\mathrm{f}i}} I_{li}(U_i) \\ \dot{I}_i = -\dfrac{R_{\mathrm{f}i}}{L_{\mathrm{f}i}} I_i - \dfrac{1}{L_{\mathrm{f}i}} U_i + \dfrac{1}{L_{\mathrm{f}i}} u_i \\ \dot{\mathscr{U}}_i = U_{\mathrm{r}i} - U_i \end{cases} \tag{1}$$

where the electrical parameters are detailed in Table II. Further, utilizing the ZIP load equivalent representation introduced in [26], the load current can be expressed as

$$I_{li}(U_i) = \left(\frac{1}{R_{li}} - \frac{P_{li}}{U_{\mathrm{r}i}^2}\right) U_i + I_{li} + \frac{2P_{li}}{U_{\mathrm{r}i}}. \tag{2}$$

Substituting (2) into the subsystem dynamics (1) yields the resulting local dynamics of DCmGs:

$$\begin{cases} \dot{U}_i = \dfrac{1}{C_{\mathrm{f}i}} I_i + \left(\dfrac{P_{li}}{C_{\mathrm{f}i}U_{ri}^2} - \dfrac{1}{R_{li}C_{\mathrm{f}i}}\right) U_i \\ \qquad - \dfrac{1}{C_{\mathrm{f}i}}\left(I_{li} + \dfrac{2P_{li}}{U_{ri}}\right) + \displaystyle\sum_{j\in\mathcal{N}_i} \frac{1}{R_{ij}C_{\mathrm{f}i}}(U_j - U_i) \\ \dot{I}_i = -\dfrac{R_{\mathrm{f}i}}{L_{\mathrm{f}i}} I_i - \dfrac{1}{L_{\mathrm{f}i}} U_i + \dfrac{1}{L_{\mathrm{f}i}} u_i \\ \dot{\mathscr{U}}_i = U_{ri} - U_i. \end{cases} \tag{3}$$

The above dynamics can be reformulated into the following linear time-invariant (LTI) state-space representation:

$$\begin{cases} \dot{x}_i(t) = A_{ii}x_i(t) + B_i u_i(t) + E_i w_i(t) \\ \qquad + A_{li}x_i(t) + \displaystyle\sum_{j\in\mathcal{N}_i} A_{ij}\big(x_j(t) - x_i(t)\big) \\ y_i(t) = D_i x_i(t) \end{cases} \tag{4}$$

where $x_i = [U_i, I_i, \mathscr{U}_i]^T$ is the state vector of subsystem i, and x_j represents the neighbor state for $i \in \mathcal{V}, j \in \mathscr{N}_i$. Moreover, y_i denotes the measured output and u_i is the control action to the power converter. $w_i = [I_{li}, \frac{2P_{li}}{U_{\mathrm{ri}}}, U_{\mathrm{ri}}]^T$ denotes external disturbances. The term $A_{li}x_i(t)$ captures the load-related effects, while $\sum_{j\in\mathscr{N}_i} A_{ij}(x_j(t)-x_i(t))$ accounts for the coupling induced by power lines. Since all electrical parameters are constant, the resulting system matrices are time-invariant, which are given by

$$A_{ii} = \begin{bmatrix} 0 & \frac{1}{C_{\mathrm{f}i}} & 0 \\ -\frac{1}{L_{\mathrm{f}i}} & -\frac{R_{\mathrm{f}i}}{L_{\mathrm{f}i}} & 0 \\ -1 & 0 & 0 \end{bmatrix},\ A_{ij} = \begin{bmatrix} \frac{1}{R_{ij}C_{\mathrm{f}i}} & 0 & 0 \\ 0 & 0 & 0 \\ 0 & 0 & 0 \end{bmatrix},$$
$$A_{li} = \begin{bmatrix} \frac{P_{li}}{C_{\mathrm{f}i}U_{\mathrm{f}i}^2} - \frac{1}{R_{li}C_{\mathrm{f}i}} & 0 & 0 \\ 0 & 0 & 0 \\ 0 & 0 & 0 \end{bmatrix},\ B_i = \begin{bmatrix} 0 \\ \frac{1}{L_{\mathrm{f}i}} \\ 0 \end{bmatrix},$$
$$E_i = \begin{bmatrix} -\frac{1}{C_{\mathrm{f}i}} & -\frac{1}{C_{\mathrm{f}i}} & 0 \\ 0 & 0 & 0 \\ 0 & 0 & 1 \end{bmatrix}, D_i = \mathbf{I}.$$

B. Polytopic Uncertain DCmG Model

In practical DCmGs, the electrical parameters of DGUs, power lines, and ZIP loads are subject to uncertainty due to internal factors like over-voltages and overheating, as well as external influences including bonding wire disruptions and hot carrier injection [27]. These uncertainties can be reasonably bounded based on empirical measurements, historical data, and industry standards. Moreover, utilities and operators continuously monitor these parameter variations in real time, establishing and updating uncertainty intervals accordingly [18]. This operational monitoring supports the assumption that system parameters remain within predefined bounds under normal conditions.

Specifically, system parameters are assumed to vary within known bounds, e.g., $0 \le \underline{R}_{\mathrm{f}i} \le R_{\mathrm{f}i} \le \overline{R}_{\mathrm{f}i}$, and similarly for power lines and ZIP loads. Inspired by polytopic uncertainty modeling techniques [28], the system matrices A_{ii}, A_{ij}, and A_{li} are assumed to lie in a convex polytopic set defined by the vertices corresponding to the extreme parameter values as

$$\begin{aligned} &[A_{ii},\ A_{ij},\ A_{li}] \in \mathbb{S} \triangleq \Bigg\{ \sum_{k=1}^{G} \theta_k = 1,\ \theta_k \ge 0, \\ &[A_{ii}(\theta), A_{ij}(\theta), A_{li}(\theta)] = \sum_{k=1}^{G} \theta_k \left[A_{ii}^k, A_{ij}^k, A_{li}^k\right] \Bigg\} \end{aligned} \tag{5}$$

where

$$A_{ii}^k = \begin{bmatrix} 0 & \frac{1}{C_{\mathrm{f}i}} & 0 \\ -\frac{1}{L_{\mathrm{f}i}} & -\frac{R_{\mathrm{f}i}^k}{L_{\mathrm{f}i}} & 0 \\ -1 & 0 & 0 \end{bmatrix},\ A_{ij}^k = \begin{bmatrix} \frac{1}{R_{ij}^k C_{\mathrm{f}i}} & \mathbf{0}^{1\times 2} \\ \mathbf{0}^{2\times 1} & \mathbf{0}^{2\times 2} \end{bmatrix},$$
$$A_{li}^k = \begin{bmatrix} \frac{P_{li}^k}{C_{\mathrm{f}i}U_{\mathrm{f}i}^2} - \frac{1}{R_{li}^k C_{\mathrm{f}i}} & \mathbf{0}^{1\times 2} \\ \mathbf{0}^{2\times 1} & \mathbf{0}^{2\times 2} \end{bmatrix},$$

and the polytopic uncertainties $R_{\mathrm{f}i}^k$, R_{li}^k, I_{li}^k, P_{li}^k, and R_{ij}^k $(k = 1, 2, \ldots, G)$ denote DGU, ZIP load and power line related parameters within the specified intervals.

It should be noted that, in rare situations where load parameters exceed the defined bounds, such as due to device malfunctions or sudden large CPLs (a part of ZIP loads), these anomalies are typically identified and handled by higher-level protection and emergency management systems, (e.g., circuit breakers). Within the defined uncertainty set relevant to normal operation, however, the relative influence of different factors is not uniform. Variations in CPLs represent the most critical source of instability owing to their nonlinear and negative impedance characteristics, whereas line parameter uncertainties exert a moderate impact that is effectively mitigated by the proposed method. In contrast, uncertainties in filter resistance play only a minor role, as they primarily affect damping. This analysis underscores the importance of developing scalable control strategies that directly address the dominant destabilizing mechanisms in DCmGs.

Therefore, a polytopic uncertain DCmG model can be formulated as follows:

$$\mathbb{T}_i : \begin{cases} \dot{x}_i(t) = \big(A_{ii}(\theta) + A_{li}(\theta)\big)x_i(t) + B_i u_i(t) \\ \qquad\quad + E_i w_i(t) + \sum\limits_{j\in\mathscr{N}_i} A_{ij}(\theta)\big(x_j(t) - x_i(t)\big) \\ y_i(t) = D_i x_i(t). \end{cases} \tag{6}$$

Remark 1: The resulting polytopic uncertain model $\mathbb{T}_i$ (6) captures a continuum of potential equilibria induced by bounded electrical parameter uncertainties within the defined polytopic set $\mathbb{S}$. To strike a balance between robustness and computational efficiency, the DGU uncertainty is primarily modeled in the filter resistance $R_{\mathrm{f}i}$, due to its sensitivity to environmental variations and its critical role in system damping. Although $L_{\mathrm{f}i}$ and $C_{\mathrm{f}i}$ are also subject to aging, their degradation occurs on a much slower time scale compared to the control dynamics studied here. In particular, a reduction of up to 20% in capacitance is commonly regarded as the end-of-life threshold. Such long-term variations are continuously monitored by utilities in practice, and aged capacitors are typically replaced before exceeding allowable limits [29]. Therefore, within the expected operational horizon, $L_{\mathrm{f}i}$ and $C_{\mathrm{f}i}$ can be reasonably assumed constant, whereas $R_{\mathrm{f}i}$ captures the dominant and faster-varying uncertainty. This modeling choice is consistent with established practices in robust control design for microgrids [18], [30], while preserving analytical tractability and ensuring robust performance over all admissible parameter variations.

Similar to work [21], the pair of system matrices $(A_{ii}(\theta), B_i)$ is controllable. Therefore, the controller of interest is designed as

$$u_i(t) = K_i x_i(t) \tag{7}$$

where $K_i = [K_{1i}, K_{2i}, K_{3i}]$ represents the multivariable proportional-integral controller gain.

Remark 2: Control strategies in DCmGs can be characterized from two complementary dimensions: hierarchical control levels and communication architecture [31]. From a hierarchical perspective, primary control is responsible for fast local voltage regulation, secondary control achieves current and power sharing, and tertiary control addresses optimization and

$$\boldsymbol{A}(\theta)=\begin{bmatrix} A_{11}(\theta)+A_{l1}(\theta)+A_{d1}(\theta) & A_{12}(\theta) & \cdots & A_{1n}(\theta) \\ A_{21}(\theta) & A_{22}(\theta)+A_{l2}(\theta)+A_{d2}(\theta) & \cdots & A_{2n}(\theta) \\ \vdots & \vdots & \ddots & \vdots \\ A_{n1}(\theta) & A_{n2}(\theta) & \cdots & A_{nn}(\theta)+A_{ln}(\theta)+A_{dn}(\theta) \end{bmatrix},$$

$$\boldsymbol{B}=\operatorname{diag}\{B_1,B_2,\ldots,B_n\},\boldsymbol{D}=\operatorname{diag}\{D_1,D_2,\ldots,D_n\},\boldsymbol{E}=\operatorname{diag}\{E_1,E_2,\ldots,E_n\},\boldsymbol{K}=\operatorname{diag}\{K_1,K_2,\ldots,K_n\}.$$

grid coordination. Meanwhile, based on the communication structure, centralized control relies on a global controller and full-system communication, but suffers from poor scalability and vulnerability to single-point failures. Distributed control improves flexibility by enabling local coordination via communication links, yet still faces challenges such as time delays, cyber risks, and privacy concerns. In contrast, the proposed fully decentralized control operates entirely without communication: each DGU calculates its local control input $u_i(t)$ using only its own electrical parameters and state measurements. Specifically, this decentralized approach offers several notable advantages [8], [32]:

(1) Scalability: The decentralized design enables subsystems to be plugged in or out with minimal changes to the local controller structure and parameters, or even without any change, while preserving system stability.
(2) Resilience: The absence of communication dependencies enhances robustness to delays and cyber-attacks.
(3) Redundancy: The architecture inherently provides redundancy for load power supplies, ensuring continued operation even in the absence of a centralized system.
(4) Simplicity: The fully local control structure facilitates implementation, making the approach practical for large-scale DCmGs.

Remark 3: Note that droop control is a widely used primary-level approach to achieve proportional power sharing among DGUs without requiring communication via virtual impedance [33], [34]. However, droop-based methods involve several trade-offs: they inherently compromise voltage regulation accuracy, require careful selection and tuning of droop coefficients and virtual impedance values [31], and substantially increase the complexity of LMI-based stability analysis when combined with polytopic uncertainty models. Moreover, as discussed in [24], the stability of droop controllers is generally guaranteed only for specific microgrid topologies or when supplemented by networked secondary controllers, which limits scalability. In contrast, the proposed decentralized dissipative control ensures robust voltage stabilization under PnP operations entirely without communication among DGUs.

C. Global DCmGs Consisting of n DGUs

As shown in the upper frame of Fig. 1, a global DCmGs denoted as $\mathbf{T}_n$ can be comprised of n subsystems $\mathbb{T}_i$, which are interconnected in a decentralized manner via power lines. The collective global DCmGs model is given by

$$\mathbf{T}_n:\begin{cases}\dot{\boldsymbol{x}}(t)=(\boldsymbol{A}(\theta)+\boldsymbol{B}\boldsymbol{K})\,\boldsymbol{x}(t)+\boldsymbol{E}\boldsymbol{w}(t)\\ \boldsymbol{y}(t)=\boldsymbol{D}\boldsymbol{x}(t)\end{cases}\tag{8}$$

where

$$\boldsymbol{x}(t)=\left[x_1^T(t),x_2^T(t),\ldots,x_n^T(t)\right]^T,$$
$$\boldsymbol{w}(t)=\left[w_1^T(t),w_2^T(t),\ldots,w_n^T(t)\right]^T,$$
$$\boldsymbol{y}(t)=\left[y_1^T(t),y_2^T(t),\ldots,y_n^T(t)\right]^T,$$

and system matrices are listed at the top of this page.

Note that the system matrix $\boldsymbol{A}(\theta)$ in (8) includes the dynamics of DGUs, power lines, and ZIP loads. Based on its structural properties, it can be decomposed as follows:

$$\boldsymbol{A}(\theta)=\boldsymbol{A}_v(\theta)+\boldsymbol{A}_l(\theta)+\boldsymbol{A}_d(\theta)+\boldsymbol{A}_a(\theta)\tag{9}$$

where the matrix $\boldsymbol{A}_v(\theta)=\operatorname{diag}\{A_{11}(\theta),A_{22}(\theta),\ldots,A_{nn}(\theta)\}$ exclusively captures the DGU dynamics without accounting for lines and loads. $\boldsymbol{A}_l(\theta)=\operatorname{diag}\{A_{l1},A_{l2},\ldots,A_{ln}\}$ only collects the polytopic uncertain information related to ZIP loads. Both components $\boldsymbol{A}_d(\theta)$ and $\boldsymbol{A}_a(\theta)$ denote the polytopic uncertain power lines. Specifically, $\boldsymbol{A}_d(\theta)=\operatorname{diag}\{A_{d1}(\theta),A_{d2}(\theta),\ldots,A_{dn}(\theta)\}$ considers the dependency of each local state on the neighboring DGUs, with each block $A_{di}(\theta)=\sum_{k=1}^{G}\theta_k A_{di}^k$, where

$$A_{di}^k=\left[\begin{array}{c|c}-\sum\limits_{j\in\mathcal{N}_i}\frac{1}{R_{ij}^k C_{\mathrm{fi}}} & \mathbf{0}^{1\times 2}\\ \hline \mathbf{0}^{2\times 1} & \mathbf{0}^{2\times 2}\end{array}\right].\tag{10}$$

Moreover, $\boldsymbol{A}_a(\theta)$ encompasses the impact of line couplings, comprising zero blocks on the diagonal and blocks $A_{ij}(\theta)$ on the off-diagonal.

Then, the following lemmas and definition are presented, which are fundamental for the stability analysis and controller design in this paper.

Lemma 1 [35]: The Laplacian matrix is symmetric and positive semidefinite.

Proof: Based on *Graph Theory* in [35], the Laplacian matrix is defined as $\mathcal{L}=\mathcal{D}-\mathcal{A}$. Here, $\mathcal{D}$ is the diagonal degree matrix, which means it is symmetric, while $\mathcal{A}$ is the adjacency matrix, which is symmetric because the graph $\mathcal{G}$ is undirected. Since both $\mathcal{D}$ and $\mathcal{A}$ are symmetric, their difference $\mathcal{L}$ is also symmetric.

Furthermore, the Laplacian matrix can be expressed as $\mathcal{L}=FF^T$, where F is the vertex-edge incidence matrix of the graph $\mathcal{G}$. For any real vector $\rho\in\mathbb{R}^n$, the following holds:

$$\rho^T\mathcal{L}\rho=\rho^T FF^T\rho=\left\|F^T\rho\right\|^2\geq 0.$$

The above quadratic form can be expanded explicitly as

$$\rho^T\mathcal{L}\rho=\sum_{(i,j)\in\mathcal{E}}a_{ij}(\rho_i-\rho_j)^2\geq 0$$

which is a sum of squares and thus non-negative for all $\rho\in\mathbb{R}^n$. It can be concluded that $\mathcal{L}$ is positive semidefinite. Therefore, $\mathcal{L}$ is symmetric and positive semidefinite, which

concludes the proof.

Definition 1 [36]: The resulting system $\mathbb{T}_i$ is said to be dissipative if there exists a non-negative storage function $V_i(x_i(t))$, analogous to a Lyapunov function, such that for all $t > t_0 \geq 0$, the following inequality holds:

$$V_i(x_i(t)) - V_i(x_i(t_0)) \leq \int_{t_0}^{t} \mathscr{F}_i(y_i(\tau), w_i(\tau))d\tau$$

where $x_i(t_0)$ represents the system's initial state and $\mathscr{F}_i(y_i(t), w_i(t))$ denotes the energy supply rate. Moreover, the system $\mathbb{T}_i$ is guaranteed to exhibit QSR-dissipativity if it is dissipative with respect to the following energy supply rate:

$$\begin{aligned}\mathscr{F}(y_i(\tau), w_i(\tau)) = y_i^T(\tau)Q_i y_i(\tau) + 2y_i^T(\tau)S_i w_i(\tau) \\ + w_i^T(\tau)R_i w_i(\tau)\end{aligned}$$

where Q_i, S_i, and R_i are appropriately dimensioned real matrices that define the dissipativity properties.

III. Problem Formulation

This section formulates the problem of dissipative stability analysis and scalable controller design for nonlinear DCmGs under PnP operations.

Lemma 2 (Centralized Dissipativity Analysis): Given a positive definite matrix $\boldsymbol{\phi} = \text{diag}\{\phi_1, \phi_2, \ldots, \phi_n\}$, the global DCmG system $\mathbf{T}_n$, incorporating uncertain DGUs, power lines and ZIP loads, is QSR-dissipative if there exist matrices $\boldsymbol{K}, \boldsymbol{S}, \boldsymbol{M}$, symmetric matrices $\boldsymbol{Q}, \boldsymbol{R}$, and a positive definite matrix $\boldsymbol{P}(\theta)$ such that the following LMI condition holds:

$$\boldsymbol{\Phi}(\theta) = \begin{bmatrix} \widehat{\boldsymbol{\Phi}} - \boldsymbol{Q} & \widetilde{\boldsymbol{\Phi}} & \boldsymbol{ME} - \boldsymbol{S} \\ * & -\boldsymbol{\phi}(\boldsymbol{M} + \boldsymbol{M}^T) & \boldsymbol{\phi ME} \\ * & * & -\boldsymbol{R} \end{bmatrix} < 0 \tag{11}$$

where

$$\begin{aligned}&\widehat{\boldsymbol{\Phi}} = \boldsymbol{MA}(\theta) + \boldsymbol{A}^T(\theta)\boldsymbol{M}^T + \boldsymbol{MBK} + \boldsymbol{K}^T\boldsymbol{B}^T\boldsymbol{M}^T, \\ &\widetilde{\boldsymbol{\Phi}} = \boldsymbol{\phi A}^T(\theta)\boldsymbol{M}^T + \boldsymbol{P}(\theta) - \boldsymbol{M} + \boldsymbol{\phi K}^T\boldsymbol{B}^T\boldsymbol{M}^T, \\ &\boldsymbol{M} = \text{diag}\{M_1, M_2, \ldots, M_n\}, \boldsymbol{Q} = \text{diag}\{Q_1, Q_2, \ldots, Q_n\}, \\ &\boldsymbol{S} = \text{diag}\{S_1, S_2, \ldots, S_n\}, \boldsymbol{R} = \text{diag}\{R_1, R_2, \ldots, R_n\}, \\ &\boldsymbol{P}(\theta) = \text{diag}\{\mathbb{P}_1(\theta), \mathbb{P}_2(\theta), \ldots, \mathbb{P}_n(\theta)\}, \\ &\mathbb{P}_i(\theta) = \sum_{k=1}^{G} \theta_k \mathbb{P}_i^k, \ \mathbb{P}_i^k > 0.\end{aligned}$$

Proof: Choose a polytopic parameter-dependent storage function as $\boldsymbol{V}(\boldsymbol{x}(t)) = \sum_{i=1}^{n} V_i(x_i(t)) = \boldsymbol{x}^T(t)\boldsymbol{P}(\theta)\boldsymbol{x}(t)$. Differentiating along the trajectories of $\mathbf{T}_n$ yields: $\dot{\boldsymbol{V}}(\boldsymbol{x}(t)) = 2\boldsymbol{x}^T(t)\boldsymbol{P}(\theta)\dot{\boldsymbol{x}}(t)$.

By utilizing the general free-weight matrix technique [28], there exist matrices $\boldsymbol{M}$ and $\boldsymbol{\phi}$ such that

$$\mathscr{Z} = 2\left[\boldsymbol{x}^T(t) + \boldsymbol{\phi}\dot{\boldsymbol{x}}(t)\right]\boldsymbol{MN} = 0 \tag{12}$$

where $\boldsymbol{N} = (\boldsymbol{A}(\theta) + \boldsymbol{BK})\boldsymbol{x}(t) + \boldsymbol{Ew}(t) - \dot{\boldsymbol{x}}(t)$.

For any bounded non-zero disturbance $\boldsymbol{w}(t)$, the performance criterion is defined as

$$J(\tau) = \int_0^\tau \begin{bmatrix} \boldsymbol{y}(t) \\ \boldsymbol{w}(t) \end{bmatrix}^T \begin{bmatrix} \boldsymbol{Q} & \boldsymbol{S} \\ * & \boldsymbol{R} \end{bmatrix}^T \begin{bmatrix} \boldsymbol{y}(t) \\ \boldsymbol{w}(t) \end{bmatrix} dt. \tag{13}$$

Under zero initial conditions, it follows that

$$\begin{aligned}J^\star =& \boldsymbol{V}(\boldsymbol{x}(\tau)) - J(\tau) = \int_0^\tau \Big\{\dot{\boldsymbol{V}}(\boldsymbol{x}(t)) + \mathscr{Z} - \boldsymbol{y}^T(t)\boldsymbol{Q}\boldsymbol{y}(t) \\ &-2\boldsymbol{y}^T(t)\boldsymbol{S}\boldsymbol{w}(t) - \boldsymbol{w}^T(t)\boldsymbol{R}\boldsymbol{w}(t)\Big\}dt \\ =& \int_0^\tau \Big\{\boldsymbol{\xi}^T(t)\boldsymbol{\Phi}(\theta)\boldsymbol{\xi}(t)\Big\}dt\end{aligned} \tag{14}$$

where $\boldsymbol{\xi}(t) = \left[\boldsymbol{x}^T(t), \dot{\boldsymbol{x}}^T(t), \boldsymbol{w}^T(t)\right]^T$.

Since $\boldsymbol{\Phi}(\theta) < 0$ in (11), it follows directly that $J^\star < 0$, confirming the QSR-dissipativity of the system $\mathbf{T}_n$ (8) according to Definition 1. This completes the proof.

Remark 4: Lemma 2 establishes a QSR-dissipativity condition for the global DCmG systems $\mathbf{T}_n$, incorporating information of DGUs, power lines, and ZIP loads. The general free-weight matrix technique (12) is employed using a fully parameterized matrix $\boldsymbol{M}$ and a user-defined tuning coefficient $\boldsymbol{\phi}$. This approach avoids product terms between the polytopic uncertainty matrix $\boldsymbol{A}(\theta)$ and the parameter-dependent storage function matrix $\boldsymbol{P}(\theta)$, significantly simplifying the stability condition. However, it lacks scalability for PnP operations, as the number of DGUs and the associated line couplings can change dynamically when DGUs are added or removed.

According to (9), $\boldsymbol{\Phi}(\theta)$ given in Lemma 2 can be decomposed into three parts as follows:

$$\boldsymbol{\Phi}(\theta) = \boldsymbol{\Phi}_v(\theta) + \boldsymbol{\Phi}_{ad}(\theta) + \boldsymbol{\Phi}_l(\theta) \tag{15}$$

where

$$\boldsymbol{\Phi}_v(\theta) = \begin{bmatrix} \widehat{\boldsymbol{\Phi}}_v - \boldsymbol{Q} & \widetilde{\boldsymbol{\Phi}}_v & \boldsymbol{ME} - \boldsymbol{S} \\ * & -\boldsymbol{\phi}(\boldsymbol{M} + \boldsymbol{M}^T) & \boldsymbol{\phi ME} \\ * & * & -\boldsymbol{R} \end{bmatrix} \tag{16a}$$

$$\boldsymbol{\Phi}_{ad}(\theta) = \left[\begin{array}{c|c|c} \widehat{\boldsymbol{\Phi}}_{ad} & \boldsymbol{\phi A}_a^T(\theta)\boldsymbol{M}^T + \boldsymbol{\phi A}_d^T(\theta)\boldsymbol{M}^T & \boldsymbol{0}^{3n\times 3n} \\ \hline * & \boldsymbol{0}^{3n\times 3n} & \boldsymbol{0}^{3n\times 3n} \\ \hline * & * & \boldsymbol{0}^{3n\times 3n} \end{array}\right] \tag{16b}$$

$$\boldsymbol{\Phi}_l(\theta) = \left[\begin{array}{c|c|c} \boldsymbol{MA}_l(\theta) + \boldsymbol{A}_l^T(\theta)\boldsymbol{M}^T & \boldsymbol{\phi A}_l^T\boldsymbol{M}^T & \boldsymbol{0}^{3n\times 3n} \\ \hline * & \boldsymbol{0}^{3n\times 3n} & \boldsymbol{0}^{3n\times 3n} \\ \hline * & * & \boldsymbol{0}^{3n\times 3n} \end{array}\right] \tag{16c}$$

with

$$\begin{aligned}&\widehat{\boldsymbol{\Phi}}_v = \boldsymbol{MA}_v(\theta) + \boldsymbol{A}_v^T(\theta)\boldsymbol{M}^T + \boldsymbol{MBK} + \boldsymbol{K}^T\boldsymbol{B}^T\boldsymbol{M}^T, \\ &\widetilde{\boldsymbol{\Phi}}_v = \boldsymbol{\phi A}_v^T(\theta)\boldsymbol{M}^T + \boldsymbol{P}(\theta) - \boldsymbol{M} + \boldsymbol{\phi K}^T\boldsymbol{B}^T\boldsymbol{M}^T, \\ &\widehat{\boldsymbol{\Phi}}_{ad} = \boldsymbol{MA}_a(\theta) + \boldsymbol{MA}_d(\theta) + \boldsymbol{A}_a^T(\theta)\boldsymbol{M}^T + \boldsymbol{A}_d^T(\theta)\boldsymbol{M}^T.\end{aligned}$$

Specifically, (16a) exclusively captures the dissipativity of DGUs. Both (16b) and (16c) denote the negative effects of power lines and ZIP loads on the dissipativity condition (11).

The dissipativity condition (11) relies on the global information about DGUs, ZIP loads, and power lines. In practice, PnP operations frequently alter both the number of DGUs and the coupling of power lines, which substantially increases computational complexity and risks transient voltage fluctuations. Therefore, it is essential to develop a scalable approach for stability analysis and controller design that can operate in conjunction with the PnP functionality. In this context, the problems considered in this paper are as follows:

1) *Decentralized dissipativity analysis:* Reformulate the cen-

tralized dissipativity condition in Lemma 2 into decentralized conditions at the individual DGU level, independently of the adverse effects stemming from uncertain power lines and ZIP loads.

2) *Scalable controller design:* Develop a local controller synthesis method requiring only DGU-specific parameters, without reliance on line coupling or ZIP load information.
3) *Seamless PnP operations:* Guarantee seamless PnP operations such that the addition or removal of a DGU does not necessitate controller re-design or grid reconfiguration, while maintaining the global dissipativity of the DCmG system.

IV. Decentralized Dissipativity Analysis and Scalable Controller Design for DCmGs

This section first examines the decentralized QSR-dissipativity of local DCmGs $\mathbb{T}_i$ (6), and then presents a localized approach to scalable controller design based on DGU dynamics.

To enable a fully decentralized-based scalable design based solely on local DGU information, it is essential to eliminate the negative effects introduced by power lines and ZIP loads. Once these adverse influences are mitigated, the dissipativity of the global DCmG system can be ensured by satisfying only the local dissipativity conditions of individual DGUs. To this end, the following assumption is introduced.

Assumption 1 (SFWM technique): Each block M_i of the free-weight matrix $\boldsymbol{M}$ in (12) is assumed to adopt the following fixed structure:

$$M_i = \left[\begin{array}{c|c} \beta_i & M_i^{12} \\ \hline \mathbf{0}^{2\times 1} & M_i^{22} \end{array}\right] \tag{17}$$

where β_i is a positive scalar, and $M_i^{12} \in \mathbb{R}^{1\times 2}, M_i^{22} \in \mathbb{R}^{2\times 2}$ are arbitrary real matrices.

Under the proposed SFWM technique, the decentralized dissipativity analysis for global DCmGs $\mathbf{T}_n$ is outlined below.

A. Decentralized Dissipativity Analysis of Local DCmGs

Theorem 1: Given a positive scalar ϕ_i and a load condition $P_{li}^k \le U_{ri}^2/R_{li}^k, k = 1, 2, \ldots, G$, the global DCmG system $\mathbf{T}_n$ with uncertainties is QSR-dissipative if there exist suitable matrices K_i, S_i, symmetric matrices Q_i, R_i, a structured matrix M_i satisfying format (17), and a positive definite matrix $\mathbb{P}_i^k$ such that the following LMI condition holds:

$$\Pi_i^k = \left[\begin{array}{ccc} \widehat{\Pi}_i^k - Q_i & \widetilde{\Pi}_i^k & M_iE_i - S_i \\ * & -\phi_i(M_i + M_i^T) & \phi_i M_i E_i \\ * & * & -R_i \end{array}\right] < 0 \tag{18}$$

where

$$\widehat{\Pi}_i^k = M_iA_{ii}^k + A_{ii}^{kT}M_i^T + M_iB_iK_i + K_i^TB_i^TM_i^T,$$
$$\widetilde{\Pi}_i^k = \phi_iA_{ii}^{kT}M_i^T + \mathbb{P}_i^k - M_i + \phi_iK_i^TB_i^TM_i^T.$$

Proof: Firstly, the convex combination of the conditions given in Theorem 1 leads to the following condition:

$$\left[\begin{array}{ccc} \widehat{\Phi}_i(\theta) - Q_i & \widetilde{\Phi}_i(\theta) & M_iE_i - S_i \\ * & -\phi_i(M_i + M_i^T) & \phi_i M_i E_i \\ * & * & -R_i \end{array}\right] < 0 \tag{19}$$

where

$$\widehat{\Phi}_i(\theta) = M_iA_{ii}(\theta) + A_{ii}^T(\theta)M_i^T + M_iB_iK_i + K_i^TB_i^TM_i^T,$$
$$\widetilde{\Phi}_i(\theta) = \phi_iA_{ii}^T(\theta)M_i^T + \mathbb{P}_i(\theta) - M_i + \phi_iK_i^TB_i^TM_i^T.$$

Further, by consolidating the above condition (19), it can be obtained that from $\boldsymbol{\Phi}_v(\theta)$ in (16a) that

$$\boldsymbol{\Phi}_v < 0 \tag{20}$$

which exclusively accounts for the DGU model.

Then, combining matrices A_{di}^k given in (10) and M_i defined in (17), the product term $\boldsymbol{M}\boldsymbol{A}_d(\theta)$ (or $\boldsymbol{A}_d^T(\theta)\boldsymbol{M}^T$) in (16b) is also block diagonal, with each block $M_iA_{di}(\theta)$ (or $A_{di}^T(\theta)M_i^T$) given by

$$M_iA_{di}(\theta) = A_{di}^T(\theta)M_i^T = \left[\begin{array}{c|c} -\sum\limits_{k=1}^{G}\theta_k \sum\limits_{j\in\mathscr{N}_i}\frac{\beta_i}{R_{ij}^kC_{fi}} & \mathbf{0}^{1\times 2} \\ \hline \mathbf{0}^{2\times 1} & \mathbf{0}^{2\times 2} \end{array}\right]. \tag{21}$$

Moreover, each block at position (i, j) in the product term $\boldsymbol{M}\boldsymbol{A}_a(\theta)$ (or $\boldsymbol{A}_a^T(\theta)\boldsymbol{M}^T$) in (16b) corresponds to the multiplication $M_iA_{ij}(\theta)$ (or $A_{ji}^T(\theta)M_j$) if $j \in \mathscr{N}_i$; otherwise, the block at that position is zero. By direct calculation with $A_{ij}(\theta)$ and M_i, it can be obtained that

$$M_iA_{ij}(\theta) = A_{ji}^T(\theta)M_j^T = \left[\begin{array}{c|c} \sum\limits_{k=1}^{G}\theta_k\frac{\beta_i}{R_{ij}^kC_{fi}} & \mathbf{0}^{1\times 2} \\ \hline \mathbf{0}^{2\times 1} & \mathbf{0}^{2\times 2} \end{array}\right]. \tag{22}$$

From (21) and (22), it is evident that only the position (1,1) elements are nonzero, with all other entries being zero. Consequently, the positive/negative definiteness of the $3n \times 3n$ matrix represented by the term $\boldsymbol{M}\boldsymbol{A}_d(\theta) + \boldsymbol{M}\boldsymbol{A}_a(\theta)$ (or $\boldsymbol{A}_d^T(\theta)\boldsymbol{M}^T + \boldsymbol{A}_a^T(\theta)\boldsymbol{M}^T$) can be equivalently assessed by considering the following $n \times n$ matrix:

$$\widehat{\mathcal{L}} = \left[\begin{array}{cccc} \mathscr{D}_{11} & \mathscr{A}_{12} & \cdots & \mathscr{A}_{1n} \\ \mathscr{A}_{21} & \mathscr{D}_{22} & \cdots & \mathscr{A}_{2n} \\ \vdots & \vdots & \ddots & \vdots \\ \mathscr{A}_{n1} & \mathscr{A}_{n2} & \cdots & \mathscr{D}_{nn} \end{array}\right] \tag{23}$$

which is derived by eliminating the last two rows and columns from each block in (21) and (22). Specifically, it can be expressed as

$$\widehat{\mathcal{L}} = \widehat{\mathcal{D}} + \mathcal{A} \tag{24}$$

where

$$\widehat{\mathcal{D}} = \text{diag}\left\{\mathscr{D}_{11}, \mathscr{D}_{22}, \ldots, \mathscr{D}_{nn}\right\},$$
$$\mathcal{A} = \left[\begin{array}{cccc} 0 & \mathscr{A}_{12} & \cdots & \mathscr{A}_{1n} \\ \mathscr{A}_{21} & 0 & \cdots & \mathscr{A}_{2n} \\ \vdots & \vdots & \ddots & \vdots \\ \mathscr{A}_{n1} & \mathscr{A}_{n2} & \cdots & 0 \end{array}\right],$$

$$\mathscr{D}_{ii} = -\sum_{k=1}^{G}\theta_k \sum_{j\in\mathscr{N}_i}\frac{\beta_i}{R_{ij}^k C_{\mathrm{fi}}},$$

$$\mathscr{A}_{ij} = \begin{cases} \sum_{k=1}^{G}\theta_k \dfrac{\beta_i}{R_{ij}^k C_{\mathrm{fi}}}, & \text{if } i\in\mathcal{V}, j\in\mathscr{N}_i \\ 0, & \text{otherwise.} \end{cases}$$

By examining the structure of the matrix $\widehat{\mathcal{D}}$, it is clear that $-\widehat{\mathcal{D}}$ aligns with the definition of the in-degree matrix $\mathcal{D}$ in graph theory. Similarly, the structure of $\mathcal{A}$ corresponds to the definition of the adjacency matrix. Thus, $-\widehat{\mathcal{L}}$ can be interpreted as a Laplacian matrix. According to Lemma 1, $\widehat{\mathcal{L}}$ is symmetric and negative semidefinite, i.e.,

$$\widehat{\mathcal{L}} \le 0. \tag{25}$$

By setting the tuning coefficient ϕ_i close to zero [23], [24], it follows from (16b) that

$$\mathbf{\Phi}_{ad}(\theta) \le 0. \tag{26}$$

Similarly, remanding the matrices $A_{li}(\theta)$ and M_i, it can be demonstrated that the product term $\boldsymbol{M}\boldsymbol{A}_l(\theta)$ (or $\boldsymbol{A}_l^T(\theta)\boldsymbol{M}^T$) in (16c) is block diagonal. Each block $M_iA_{li}(\theta)$ (or $A_{li}(\theta)M_i^T$) is represented as

$$M_iA_{li}(\theta) = A_{li}^T(\theta)M_i^T = \left[\begin{array}{c|c} -\frac{\beta_i}{C_{\mathrm{fi}}}\sum_{k=1}^{G}\theta_k(\frac{1}{R_{li}^k}-\frac{P_{li}^k}{U_{ri}^2}) & \mathbf{0}^{1\times 2} \\ \hline \mathbf{0}^{2\times 1} & \mathbf{0}^{2\times 2} \end{array}\right]. \tag{27}$$

Evidently, matrix above has only one nonzero value located at $(1,1)$, with all other positions filled with zeros. Define matrix $\mathcal{G}_{\text{load}}$ is constructed as a collection of nonzero value, yielding

$$\mathcal{G}_{\text{load}} = \text{diag}\left\{\mathcal{G}_{l1}, \mathcal{G}_{l2}, \ldots, \mathcal{G}_{ln}\right\} \tag{28}$$

where $\mathcal{G}_{li} = -\frac{\beta_i}{C_{\mathrm{fi}}}\sum_{k=1}^{G}\theta_k(\frac{1}{R_{li}^k}-\frac{P_{li}^k}{U_{ri}^2})$. Given $\beta_i>0$, $C_{\mathrm{fi}}>0$, and the load condition $P_{li}^k \le U_{\mathrm{ri}}^2/R_{li}^k$, it follows that $\mathcal{G}_{\text{load}} \le 0$. By setting the tuning coefficient ϕ_i close to zero, one has

$$\mathbf{\Phi}_l(\theta) \le 0. \tag{29}$$

Finally, based on (29), (26), and (20), it follows that $\mathbf{\Phi}(\theta) = \mathbf{\Phi}_v(\theta) + \mathbf{\Phi}_l(\theta) + \mathbf{\Phi}_{ad}(\theta) < 0$. The proof is completed.

Remark 5: The SSF method [23]–[26] eliminates the adverse effects of power line couplings, but often results in conservatism and high computational complexity due to the block-diagonal constraints on the storage matrix and the presence of product terms between $\boldsymbol{A}(\theta)$ and $\boldsymbol{P}(\theta)$. To overcome these limitations, a SFWM approach is proposed, where the structure matrix M_i is defined in (17), and the scalar ϕ_i acts as a user-defined tuning parameter. By setting ϕ_i sufficiently close to zero [23], [24], the influence of line couplings (i.e., $\mathbf{\Phi}_{ad}(\theta)$) and ZIP loads (i.e., $\mathbf{\Phi}_l(\theta)$) can be significantly suppressed, thus simplifying the associated LMI constraints. Furthermore, the scalability of the proposed method is not highly sensitive to the exact numerical values within M_i, provided its block structure is preserved.

Remark 6: Traditional stability analysis techniques, such as input-to-state stability (ISS) analysis [37], provide rigorous tools for assessing DCmG stability. However, their direct application to large-scale DCmGs with frequent PnP operations, polytopic uncertainties in DGUs, and ZIP loads may result in conservative or numerically intractable LMI conditions. Lyapunov-based dissipativity theory offers distinct advantages in this context. First, it inherently exploits the compositional structure of DCmGs by characterizing the energy exchange of each DGU and guaranteeing global stability through their interconnection, thereby ensuring scalability to large networks. Second, dissipativity introduces supply rates as additional design variables, which, when integrated with the SFWM approach (see Assumption 1), alleviate conservatism and enhance the feasibility of SSF-based control design [23]–[26]. Consequently, dissipativity provides a systematic and computationally efficient framework well suited for uncertain and dynamically reconfigurable DCmGs.

Due to the complexity of condition (18) in Theorem 1, it is not feasible to directly parameterize the controller gain K_i using the results of Theorem 1. This limitation motivates the derivation of an alternative approach, as outlined in the following theorem.

B. Scalable Controller Design

Theorem 2: Given a positive scalar ϕ_i and a load condition $P_{li}^k \le U_{ri}^2/R_{li}^k$, $k=1,2,\ldots,G$, local subsystem $\mathbb{T}_i$ is QSR-dissipative if there exist positive scalars ζ_i, δ_i, suitable matrices $\mathcal{X}_i, \mathcal{S}_i$, symmetric matrices $\mathcal{Q}_i, \mathcal{R}_i$, a structured matrix $\mathcal{Y}_i$, and a positive definite matrix $\mathcal{P}_i^k$ such that the following local conditions hold:

$$\begin{bmatrix} \widehat{\Xi}_i^k - \mathcal{Q}_i & \widetilde{\Xi}_i^k & E_i\mathcal{Y}_i - \mathcal{S}_i \\ * & -\phi_i(\mathcal{Y}_i+\mathcal{Y}_i^T) & \phi_iE_i\mathcal{Y}_i \\ * & * & -\mathcal{R}_i \end{bmatrix} < 0 \tag{30}$$

$$\begin{bmatrix} -\zeta_i I & \mathcal{X}_i^T \\ * & -I \end{bmatrix} < 0 \tag{31}$$

$$\begin{bmatrix} \mathcal{Y}_i+\mathcal{Y}_i^T & \mathbf{1}_3 \\ * & \frac{\delta_i}{2} \end{bmatrix} > 0 \tag{32}$$

where

$$\widehat{\Xi}_i^k = A_{ii}^k\mathcal{Y}_i + \mathcal{Y}_i^TA_{ii}^{kT} + B_i\mathcal{X}_i + \mathcal{X}_i^TB_i^T,$$
$$\widetilde{\Xi}_i^k = \phi_i\mathcal{Y}_i^TA_{ii}^{kT} + \phi_i\mathcal{X}_i^TB_i^T + \mathcal{P}_i^k - \mathcal{Y}_i.$$

Then, the controller gain K_i can be parameterized as

$$K_i = \mathcal{X}_i\mathcal{Y}_i^{-1} \tag{33}$$

and is subject to the norm constraint

$$\|K_i\|_2 < \zeta_i\delta_i. \tag{34}$$

Proof: First, we denote

$$\mathcal{Q}_i = \mathcal{Y}_iQ_i\mathcal{Y}_i, \mathcal{S}_i = \mathcal{Y}_iS_i\mathcal{Y}_i, \mathcal{R}_i = \mathcal{Y}_iR_i\mathcal{Y}_i,$$
$$\mathcal{P}_i^k = \mathcal{Y}_i\mathbb{P}_i^k\mathcal{Y}_i, \mathcal{X}_i = K_i\mathcal{Y}_i, \mathcal{Y}_i^TM_i = \mathbf{I}.$$

According to $\mathcal{Y}_i^TM_i = \mathbf{I}$ and Eq. 17, one has

$$\mathcal{Y}_i = \left[\begin{array}{c|c} \overline{\beta}_i & \mathbf{0}^{1\times 2} \\ \hline \mathcal{Y}_{21i} & \mathcal{Y}_{22i} \end{array}\right] \tag{35}$$

where $\overline{\beta}_i = \beta_i^{-1}$ is a positive scalar, $\mathcal{Y}_{21i} = M_{12i}^{-T} \in \mathbb{R}^{2\times 1}$ and $\mathcal{Y}_{22i} = M_{22i}^{-T} \in \mathbb{R}^{2\times 2}$ denote the arbitrary matrices.

Then, by introducing the block diagonal matrix $\mathscr{Y}_i = \text{diag}\{\mathcal{Y}_i, \mathcal{Y}_i, \mathcal{Y}_i\}$, we perform pre-multiplication by $\mathscr{Y}_i^T$ and post-multiplication by $\mathscr{Y}_i$ on (18). This manipulation directly yields the LMI-based condition (30).

Finally, to prevent $\|K_i\|_2$ from being so large that it adversely affects the performance of DCmGs, the following constraints are taken into account:

$$\|\mathcal{X}_i\|_2 < \zeta_i \tag{36}$$

and

$$\left\|\mathcal{Y}_i^{-1}\right\|_2 < \delta_i. \tag{37}$$

By using Schur complement to the above constraints (36) and (37), LMI conditions (31) and (32) are derived. This completes the proof.

To facilitate the implementation of the proposed control method, Algorithm 1 outlines the step-by-step procedure for designing scalable dissipative voltage controllers.

Algorithm 1 Procedure for Designing Scalable Dissipative Voltage Controllers

Input: The polytopic uncertain subsystem $\mathbb{T}_i$ (6) incorporating uncertain power lines and ZIP loads.

Output: Scalable dissipative voltage controller gain K_i.

1: Specify filter parameters $R_{\text{f}i}^k$, $L_{\text{f}i}$, and $C_{\text{f}i}$, and derive the system matrices A_{ii}^k, B_i, and E_i for the polytopic local subsystem $\mathbb{T}_i$.
2: Identify the decision variables in LMIs in Theorem 2, including $\mathcal{Q}_i$, $\mathcal{S}_i$, $\mathcal{R}_i$, $\mathcal{X}_i$, $\mathcal{P}_i^k$, and the structured matrix $\mathcal{Y}_i$ conforming to (35). Solve LMIs (30), (31), and (32) using YALMIP to obtain matrices $\mathcal{X}_i$ and $\mathcal{Y}_i$.
3: If the solution in the previous step is feasible, compute the gain K_i as $K_i = \mathcal{X}_i\mathcal{Y}_i^{-1}$ based on (33).

Remark 7: The LMI conditions (30), (31), and (32) in Theorem 2 rely only on their local parameters, independent of power lines, ZIP loads, and other subsystems. The constrained parameters ζ_i in (31) and δ_i in (32) restrict the 2-norm of the controller gain to prevent excessive aggressiveness. Notably, local controllers are computed using the interface YALMIP in MATLAB [38] and semidefinite programming (SDP) solvers such as MOSEK [39] and SDPT3 [40]. Unlike previous methods [23]–[26], where numerical infeasibility of LMIs might impede PnP operations, the proposed approach enhances the solvability of the controller design and enables scalability for PnP operations. Since the number of vertices G grows linearly with the number of uncertain parameters, and each LMI is checked independently at the vertex level, the computational complexity increases moderately and remains manageable for practical applications.

Remark 8: Note that the plug-in or plug-out operation of a DGU merely results in the augmentation or reduction of the corresponding set of LMI conditions given in (30)–(32), without necessitating any modifications to the existing controllers or reconfiguration of the network. This inherent scalability ensures full compliance with privacy constraints, rendering the proposed method well-suited for energy markets characterized by heterogeneous DGU ownership. Importantly, stakeholders are not required to reveal internal system models or modify existing configurations when incorporating new DGUs into the microgrid.

Remark 9 (Seamless PnP Operations): Consider an interconnected dissipative DCmG $\mathbf{T}_n$ equipped with scalable controllers $\boldsymbol{K} = \text{diag}\{K_1, K_2, \ldots, K_n\}$, where the local controllers K_i designed using Algorithm 1, When a new system $\mathbb{T}_{n+1}$ is integrated into $\mathbf{T}_n$, the resulting system, denoted as $\mathbf{T}_{n+1} \triangleq \mathbf{T}_n|\mathbb{T}_{n+1}$, retains dissipativity provided that the local controller K_{n+1} is derived through Algorithm 1. This ensures seamless integration without disrupting the dissipative properties of the network. Furthermore, the disconnection of a subsystem is straightforward and smooth, as it does not necessitate adjustments to the controllers of the remaining units. Specifically, for the system $\mathbf{T}_n$ governed by scalable controllers $\boldsymbol{K}$, the direct removal of an existing subsystem results in the reduced system $\mathbf{T}_{n-1} \triangleq \mathbf{T}_n|\mathbb{T}_{n-1}$. The dissipativity of $\mathbf{T}_{n-1}$ is preserved, as the local controller K_{n-1} relies solely on the individual DGU model, ensuring stability without additional modifications.

V. Simulation Results

In this section, the effectiveness of the proposed method is validated through realistic computer-based simulations conducted with the Specialized Power Systems Toolbox of Simulink, which also serves as the platform for analysing quantitative performance metrics such as convergence speed and overshoot. As illustrated in Fig. 2, the considered DCmG topology consists of six DGUs, each interfaced through a bidirectional buck converter modeled using nonideal IGBT switches operating at 15kHz. The parameters of the RLC filters and the voltage reference values are listed in Table III [24]–[26]. For all DGUs, the user-defined tuning coefficient ϕ_i is set to 10^{-3}, ensuring both LMI feasibility and acceptable transient performance. In addition, ZIP loads are introduced with polytopic uncertainties in the constant impedance components, specifically: $R_{l1}^k = 4.5 \pm 1\Omega$, $R_{l2}^k = 3 \pm 1\Omega$, $R_{l3}^k = 4 \pm 1\Omega$, $R_{l4}^k = 2 \pm 1\Omega$, $R_{l5}^k = 3 \pm 1\Omega$, and $R_{l6}^k = 4 \pm 1\Omega$. The constant power components are given as: $P_{l1}^k = 300 \pm 100$W, $P_{l2}^k = 400 \pm 100$W, $P_{l3}^k = 300 \pm 100$W, $P_{l4}^k = 600 \pm 200$W, $P_{l5}^k = 400 \pm 100$W, and $P_{l6}^k = 450 \pm 100$W, for all $k = 1, 2$. These load configurations satisfy the condition $P_{li}^k \leq U_{\text{r}i}^2/R_{li}^k$.

TABLE III
Electrical Parameters for DGU i, $i = \{1, 2, \ldots, 6\}$

DGU i	$R_{\text{f}}(\Omega)$	L_{f}(mH)	C_{f}(mF)	U_{r}(V)
1	0.2	1.8	2.2	47
2	0.3	2.0	1.9	48
3	0.1	2.2	1.7	45
4	0.5	3.0	2.5	50
5	0.4	1.2	2.0	46
6	0.6	2.5	3.0	49

Using the specified parameters, the local controller gains K_i for $i = 1, 2, \ldots, 6$ are derived using YALMIP as an interface and SDP solver MOSEK through Algorithm 1, with the computed values presented in Table IV.

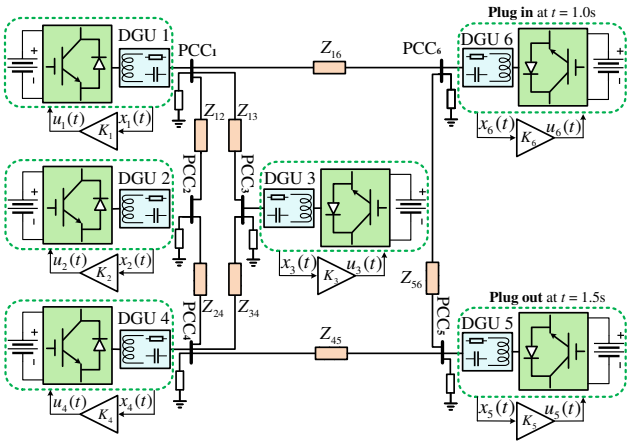

Fig. 2. Topology structure of the considered DCmGs.

TABLE IV

LOCAL CONTROLLER GAIN K_i OF DGU i

DGU i	Local controller gain K_i		
1	-0.5306	-0.1908	63.0217
2	-0.4085	-0.1579	62.1556
3	-1.8594	-0.5901	80.8392
4	-1.2105	-0.2853	98.0179
5	-0.1863	-0.1006	81.0038
6	-2.6004	-0.1895	89.0185

A. Case 1: Open-Loop Performance Without Controller

To rigorously demonstrate the necessity of the proposed control strategy, this subsection investigates the open-loop voltage tracking performance, characterized by the voltage deviation $U_{ri} - U_i$.

As illustrated in Fig. 3, in the absence of any control mechanism, the DCmG system exhibits substantial voltage fluctuations and sustained oscillations. Prior studies, such as [21], report that power semiconductor devices, including IGBTs and MOSFETs employed in power converters, are considered the most failure-prone components by approximately 34% of manufacturers. Therefore, such severe voltage deviations can impose excessive electrical and thermal stress on these components, thereby increasing the risk of device failure and compromising the DCmG reliability.

These results highlight the critical need for an advanced control framework capable of mitigating the adverse effects of PnP operations involving DGUs with ZIP loads. The subsequent case studies further validate the effectiveness of the proposed strategy in enhancing voltage regulation and ensuring robust system performance.

B. Case 2: Scalability During Plugging-in/-out Operations

This case evaluates the scalability of the proposed control method in response to network structural variations during PnP operations of DGUs.

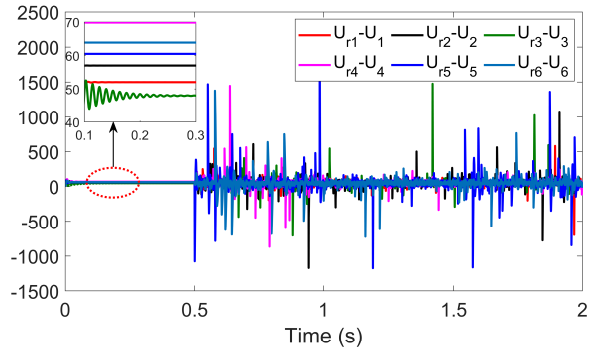

Fig. 3. Open-loop performance of voltage tracking $U_{ri} - U_i$ at PCCs.

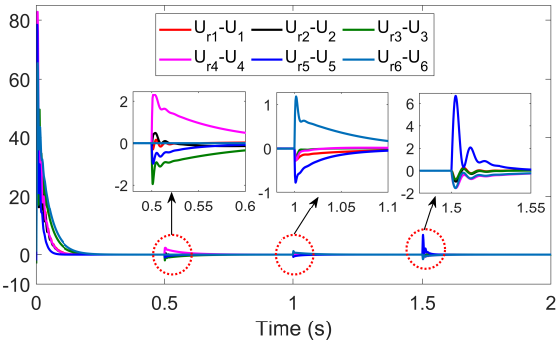

(a) Voltage tracking $U_{ri} - U_i$ at PCCs.

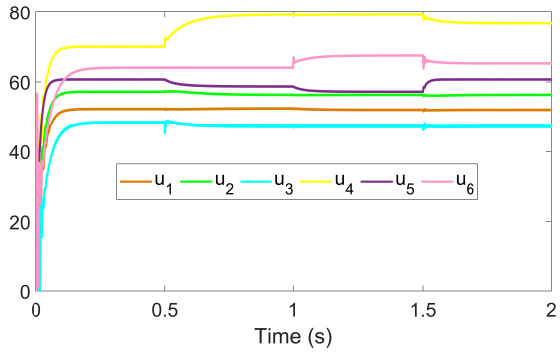

(b) Control input u_i of DGUs.

Fig. 4. Scalability performance of the proposed control scheme to PnP operations, with the connection of DGU 6 at $t = 1.0$ s and disconnection of DGU 5 at $t = 1.5$ s.

At $t = 0$ s, all interconnecting power lines are disconnected, isolating DGUs 1–6 and preventing power exchange. In this configuration, each DGU independently maintains its PCC voltage at the desired reference value U_{ri}, demonstrating autonomous voltage regulation. At $t = 0.5$ s, DGUs 1–5 are interconnected to form the microgrid topology $\mathbf{T}_5$, while DGU 6 remains isolated. Subsequently, at $t = 1.0$ s, DGU 6 is suddenly plugged into the network, and at $t = 1.5$ s, DGU 5 is abruptly disconnected. As illustrated in Fig. 4(a), only small voltage deviations (i.e., minimal overshoot) are observed during these operations, and the system quickly regains stability, indicating fast convergence. Fig. 4(b) further confirms the scalability and robustness of the proposed controller, as the control inputs u_i remain stable and uniformly bounded throughout these dynamic transitions. The specific quantitative analysis is deferred to Case 5 for comparative evaluation.

Note that at $t = 0.5$ s, the voltage tracking of DGU 6

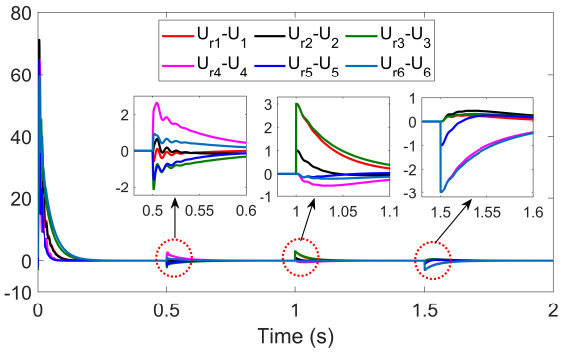

(a) Voltage tracking $U_{ri} - U_i$ at PCCs.

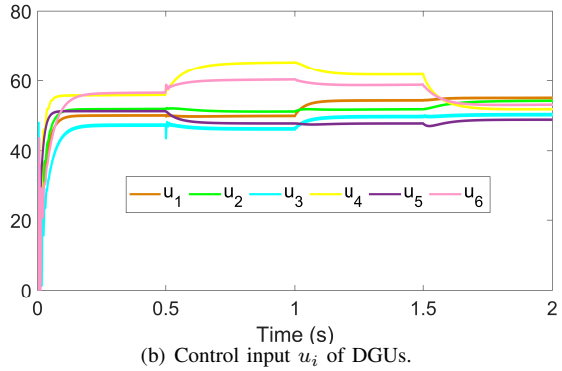

(b) Control input u_i of DGUs.

Fig. 5. Robustness of the control scheme to varying voltage references, with increases occurring at $t = 1.0$ s and decreases at $t = 1.5$ s.

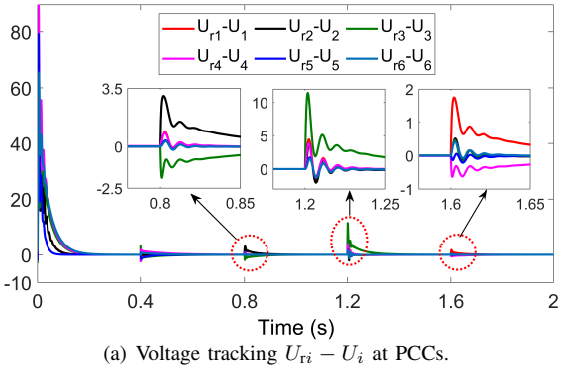

(a) Voltage tracking $U_{ri} - U_i$ at PCCs.

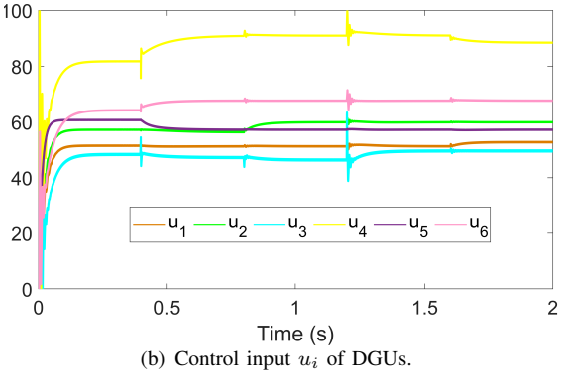

(b) Control input u_i of DGUs.

Fig. 6. Robustness of the control scheme to varying ZIP loads, with changes in electrical parameters occurring at $t = 0.8$ s, $t = 1.2$ s, and $t = 1.6$ s.

remains unaffected as it has not yet been integrated into the network, demonstrating its capability for autonomous islanded operation. This also explains the continued presence of the signal from DGU 5 after its disconnection.

C. Case 3: Robustness to Varying Voltage References

This case examines the robustness of the proposed control strategy in response to dynamic changes in voltage references.

At $t = 0.5$ s, DGUs 1–6 are interconnected to establish the DCmG topology $\mathbf{T}_6$. At $t = 1.0$ s, the voltage referencs are modified as follows: U_{r1} is increased to 50, U_{r3} to 48, and U_{r5} to 49. Subsequently, at $t = 1.5$ s, U_{r2} is decreased to 45, U_{r4} to 47, and U_{r6} to 46. Fig. 5(a) shows the PCC voltage tracking signals, while Fig. 5(b) presents the associated control inputs. These results confirm that the proposed control strategy ensures voltage stability, demonstrating strong robustness in managing dynamic reference changes.

D. Case 4: Robustness to Changing ZIP Loads

This case investigates the robustness of the proposed control framework under dynamic changes in ZIP load parameters.

At $t = 0.4$ s, DGUs 1–6 are interconnected to form the microgrid system $\mathbf{T}_6$ under the proposed local controllers. At $t = 0.8$ s, $t = 1.2$ s, and $t = 1.6$ s, the electrical parameters of ZIP loads (i.e., impedance, current, and power) are varied within their predefined uncertainty ranges. The voltage tracking performance and corresponding control inputs are depicted in Fig. 6(a) and (b). The results confirm that the proposed control strategy maintains effective voltage regulation despite load variations, highlighting its robustness under uncertain and time-varying load conditions.

E. Case 5: Comparative Analysis With Existing Methods

To provide a comprehensive evaluation of the proposed scalable voltage control strategy, comparative simulations are conducted with three representative benchmark approaches: 1) the fully free matrix method (i.e., without structured constraints in designing the free-weight matrix $\boldsymbol{M}$), 2) the SSF-based scalable decentralized control approach developed in [24], and 3) the neural network-based adaptive control from [25]. The voltage tracking results are depicted in Fig. 7(a), (b), and (c), respectively. During the initial system setup and interconnection of DGUs 1–5, all methods maintain voltage regulation with varying accuracy. However, performance disparities become evident during dynamic PnP operations. The fully free matrix method fails to ensure stability upon DGU integration and disconnection, resulting in large voltage fluctuations and divergence. The approaches in [24] and [25] maintain voltage stability but suffer from greater overshoot and slower convergence than the proposed method shown in Fig. 4(a).

To quantitatively support these observations, Table V presents a comparative summary of convergence time and voltage overshoot for each operational condition. During plug-in events, the proposed method achieves a minimum convergence time of 0.2 s and limits voltage overshoot to 2.41%, demonstrating superior transient performance. In contrast, during plug-out operations, it exhibits even faster convergence, with a response time as low as 0.1 s, while keeping voltage overshoot within 14.5%. Moreover, unlike [24] and [25], which require controller re-tuning or re-design upon topology changes, the proposed method employs pre-designed local controllers that

TABLE V
QUANTITATIVE ANALYSIS BETWEEN THE PERFORMANCE OF THE PROPOSED METHOD AND THE EXISTING METHODS

Method \ Operation condition & states	System initialization		DGUs 1–5 are interconnected		DGU 6 is plugged-in		DGU 5 is plugged-out	
	Convergence speed	Voltage overshoot	Convergence speed	Voltage overshoot	Convergence speed	Voltage overshoot	Convergence speed	Voltage overshoot
Fully free matrix method	0.3	168.96%	0.2	26.67%	divergence	–	divergence	–
Existing method [24]	1.9	182.67%	0.9	14.85%	2	14.76%	1	43.65
Existing method [25]	0.4	169.32%	0.7	4.58%	0.8	21.43%	0.5	99.78%
The proposed method	0.3	165.57%	0.2	4.5%	0.2	2.41%	0.1	14.5%

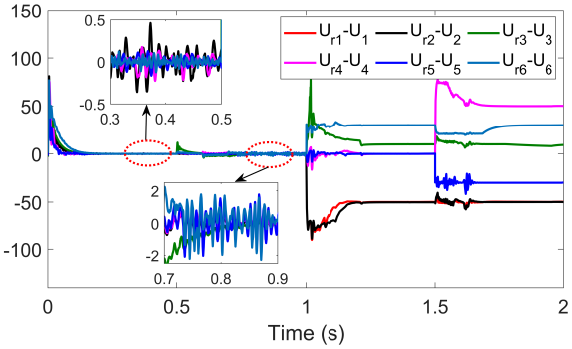

(a) Voltage tracking at PCCs using the fully free matrix method.

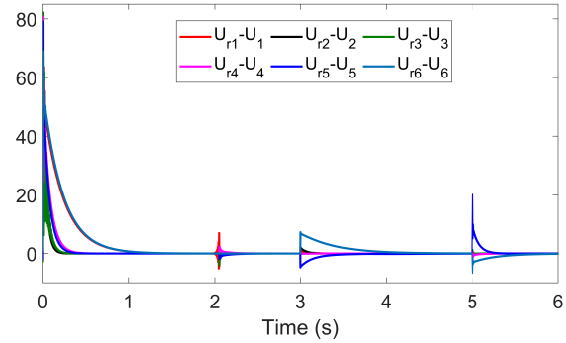

(b) Voltage tracking at PCCs using the control method in [24].

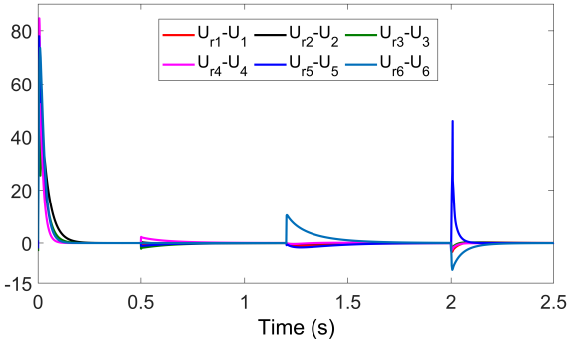

(c) Voltage tracking at PCCs using the control method in [25].

Fig. 7. Comparative analysis with three representative benchmark approaches under PnP operations.

remain valid regardless of network configuration. This feature significantly reduces computational overhead and enhances practical scalability.

Across all tested scenarios, the proposed strategy consistently outperforms the benchmark methods in both dynamic responsiveness and voltage regulation accuracy.

VI. CONCLUSION

This paper has presented a scalable dissipative voltage control approach for uncertain DCmGs with ZIP loads, enabling seamless PnP operations of DGUs. A unified polytopic DCmG model was constructed to simultaneously capture parametric uncertainties in DGUs, power lines, and ZIP loads. A SFWM technique was introduced, resulting in less conservative LMI conditions that are locally solvable. The proposed method offers the following key strengths: (i) guaranteed robust stability under polytopic uncertainties, (ii) fully localized control design independent of network topology, and (iii) plug-in/-out operations without the need for control redesign or network reconfiguration. These features were validated through comprehensive simulations, demonstrating faster convergence and reduced voltage overshoot.

While this study focused on establishing a scalable dissipativity-based framework, further sensitivity analyses would provide deeper insights into robustness under uncertainties. Future work will therefore investigate eigenvalue trajectories, pole-zero maps, and phase margin variations under different parameters, as well as robustness evaluations based on H_∞ norms.

REFERENCES

[1] M. Liu, F. Teng, Z. Zhang, P. Ge, M. Sun, R. Deng, P. Cheng, and J. Chen, "Enhancing cyber-resiliency of DER-based smart grid: A survey," *IEEE Trans. Smart Grid*, vol. 15, no. 5, pp. 4998–5030, Sep. 2024.

[2] Y. Yu, G. -P. Liu, Y. Huang, and J. M. Guerrero, "Coordinated predictive secondary control for DC microgrids based on high-order fully actuated system approaches," *IEEE Trans. Smart Grid*, vol. 15, no. 1, pp. 19–33, Jan. 2024.

[3] Z. Zhang, Y. Zhang, D. Yue, C. Dou, L. Ding, and D. Tan, "Voltage regulation with high penetration of low-carbon energy in distribution networks: A source-grid-load-collaboration-based perspective," *IEEE Trans. Ind. Inform.*, vol. 18, no. 6, pp. 3987–3999, Jun. 2022.

[4] L. Ding, Q. -L. Han, L. Y. Wang, and E. Sindi, "Distributed cooperative optimal control of DC microgrids with communication delays," *IEEE Trans. Ind. Inform.*, vol. 14, no. 9, pp. 3924–3935, Sep. 2018.

[5] M. Liu, C. Zhao, Z. Zhang, R. Deng, P. Cheng, and J. Chen, "Converter-based moving target defense against deception attacks in DC microgrids," *IEEE Trans. Smart Grid*, vol. 13, no. 5, pp. 3984–3996, Sep. 2022.

[6] X. Hu, C. Peng, H. Shen, and E. Tian, "Extended dissipative scalable control for AC islanded microgrids," *IEEE Trans. Circuits Syst. I-Regul. Pap.*, vol. 70, no. 12, pp. 5421–5432, Dec. 2023.

[7] J. Su, K. Li, and C. Xing, "Plug-and-play of grid-forming units in DC microgrids assisted with power buffers," *IEEE Trans. Smart Grid*, vol. 15, no. 2, pp. 1213–1226, Mar. 2024.

[8] T. Dragičević, X. Lu, J. C. Vasquez, and J. M. Guerrero, "DC microgrids–Part II: A review of power architectures, applications, and standardization issues," *IEEE Trans. Power Electron.*, vol. 31, no. 5, pp. 3528–3549, May 2016.

[9] B. Fan, J. Peng, Q. Yang, and W. Liu, "Distributed control of DC microgrids with improved ZIP load adaptability," *IEEE Trans. Syst. Man Cybern. -Syst.*, vol. 52, no. 7, pp. 4623–4633, Jul. 2022.

[10] J. Ferguson, M. Cucuzzella, and J. M Scherpen, "Increasing the region of attraction in DC microgrids," *Automatica*, 151, May 2023, Art. no. 110883.

[11] P. Kundur, *Power System Control and Stability*. New York: McGraw, 1994.

[12] F. Ornelas-Tellez, J. J. Rico-Melgoza, E. Espinosa-Juarez, and E. N. Sanchez, "Optimal and robust control in DC microgrids," *IEEE Trans. Smart Grid*, vol. 9, no. 6, pp. 5543–5553, Nov. 2018.

[13] X. Li, L. Guo, S. Zhang, C. Wang, Y. W. Li, A. Chen, and Y. Feng, "Observer-based DC voltage droop and current feed-forward control of a DC microgrid," *IEEE Trans. Smart Grid*, vol. 9, no. 5, pp. 5207–5216, Sep. 2018.

[14] X. Xu, Q. Liu, C. Zhang, and Z. Zeng, "Prescribed performance controller design for DC converter system with constant power loads in DC microgrid," *IEEE Trans. Syst. Man Cybern. -Syst.*, vol. 50, no. 11, pp. 4339–4348, Nov. 2020.

[15] L. Herrera, W. Zhang, and J. Wang, "Stability analysis and controller design of DC microgrids with constant power loads," *IEEE Trans. Smart Grid*, vol. 8, no. 2, pp. 881–888, Mar. 2017.

[16] F. Yang, X. Xie, and C. Peng, "Co-design of new fuzzy switching-type state-FDI estimation and attack compensation for DC microgrids under hybrid attacks," *IEEE Trans. Fuzzy Syst.*, vol. 32, no. 4, pp. 1743–1755, Apr. 2024.

[17] G. Mustafa, F. Ahmad, R. Zhang, E. U. Haq, and M. Hussain, "Adaptive sliding mode control of buck converter feeding resistive and constant power load in DC microgrid," *Energy Rep.*, vol. 9, pp. 1026–1035, Mar. 2023.

[18] J. Liu, W. Zhang, and G. Rizzoni, "Robust stability analysis of DC microgrids with constant power loads," *IEEE Trans. Power Syst.*, vol. 33, no. 1, pp. 851–860, Jan. 2018.

[19] I. Kouveliotis-Lysikatos, D. I. Koukoula, A. L. Dimeas, and N. D. Hatziargyriou, "Plug-and-play algorithms for the efficient coordination of active distribution grids," *Proc. IEEE*, vol. 110, no. 12, pp. 1927–1939, Dec. 2022.

[20] F. Boem, R. Carli, M. Farina, G. Ferrari-Trecate, and T. Parisini, "Distributed fault detection for interconnected large-scale systems: A scalable plug & play approach," *IEEE Trans. Control Netw. Syst.*, vol. 6, no. 2, pp. 800–811, Jun. 2019.

[21] A. Wang, M. Fei, and Y. Song, "A novel scalable and reliable control for DC microgrids with varying number of agents," *IEEE Trans. Cybern.*, vol. 54, no. 9, pp. 4962–4972, Sep. 2024.

[22] D. P. Guralnik, P. F. Stiller, F. M. Zegers, and W. E. Dixon, "Plug-and-play cooperative navigation: From single-agent navigation fields to graph-maintaining distributed MAS controllers," *IEEE Trans. Autom. Control*, vol. 69, no. 8, pp. 5262–5277, Aug. 2024.

[23] S. Riverso, F. Sarzo, and G. Ferrari-Trecate, "Plug-and-play voltage and frequency control of islanded microgrids with meshed topology," *IEEE Trans. Smart Grid*, vol. 6, no. 3, pp. 1176–1184, May 2015.

[24] M. Tucci, S. Riverso, J. C. Vasquez, J. M. Guerrero, and G. Ferrari-Trecate, "A decentralized scalable approach to voltage control of DC islanded microgrids," *IEEE Trans. Control Syst. Technol.*, vol. 24, no. 6, pp. 1965–1979, Nov. 2016.

[25] A. Wang, M. Fei, D. Du, C. Peng, and K. Li, "Scalable neural network control for nonlinear DC microgrids under plug-and-play operations," *IEEE Trans. Ind. Inform.*, vol. 21, no. 5, pp. 3849–3859, May 2025.

[26] P. Nahata, R. Soloperto, M. Tucci, A. Martinelli, and G. Ferrari-Trecate, "A passivity-based approach to voltage stabilization in DC microgrids with ZIP loads," *Automatica*, vol. 113, Mar. 2020, Art. no. 108770.

[27] H. Wang, M. Liserre, and F. Blaabjerg, "Toward reliable power electronics: Challenges, design tools, and opportunities," *IEEE Ind. Electron. Mag.*, vol. 7, no. 2, pp. 17–26, Jun. 2013.

[28] Y. He, M. Wu, J. She, and G. -P. Liu, "Parameter-dependent Lyapunov functional for stability of time-delay systems with polytopic-type uncertainties," *IEEE Trans. Autom. Control*, vol. 49, no. 5, pp. 828–832, May 2004.

[29] P. Saha, S. Dey, and M. Khanra, "Second-life applications of supercapacitors: Effective capacitance prognosis and aging," *J. Power Sources*, vol. 496, Jun. 2021, Art. no. 229824.

[30] J. Martínez, S. Babic, and C. Akyel, "On evaluation of inductance, DC resistance, and capacitance of coaxial inductors at low frequencies," *IEEE Trans. Magn.*, vol. 50, no. 7, pp. 1–12, Jul. 2014.

[31] T. Dragičević, X. Lu, J. C. Vasquez, and J. M. Guerrero, "DC microgrids–Part I: A review of control strategies and stabilization techniques," *IEEE Trans. Power Electron.*, vol. 31, no. 7, pp. 4876–4891, Jul. 2016.

[32] A. Wang, M. Fei, Y. Song, D. Du, C. Peng, and K. Li, "Scalable fuzzy control for nonlinear DC microgrids under plug-and-play Operations," *IEEE Trans. Fuzzy Syst.*, vol. 32, no. 8, pp. 4747–4758, Aug. 2024.

[33] A. M. Abouassy, H. Alafnan, D. -E. A. Mansour, A. Albaker, and T. F. Megahed, "An improved droop-based adaptive virtual impedance for accurate power sharing among multiple DGs in islanded microgrid," *IEEE Access*, vol. 13, pp. 108918–108933, Jun. 2025.

[34] B. Fan, Q. Li, W. Wang, G. Yao, H. Ma, X. Zeng, and J. M. Guerrero, "A novel droop control strategy of reactive power sharing based on adaptive virtual impedance in microgrids," *IEEE Trans. Ind. Electron.*, vol. 69, no. 11, pp. 11335–11347, Nov. 2022.

[35] R. Merris, "Laplacian matrices of graphs: A survey," *Linear Alg. Appl.*, vol. 197–198, pp. 143–176, Jan.–Feb. 1994.

[36] E. Agarwal, S. Sivaranjani, V. Gupta, and P. J. Antsaklis, "Distributed synthesis of local controllers for networked systems with arbitrary interconnection topologies," *IEEE Trans. Autom. Control*, vol. 66, no. 2, pp. 683–698, Feb. 2021.

[37] Y. Li, Z. Zhang, T. Dragičević, and J. Rodriguez, "A unified distributed cooperative control of DC microgrids using consensus protocol," *IEEE Trans. Smart Grid*, vol. 12, no. 3, pp. 1880–1892, May 2021.

[38] J. Lofberg, "YALMIP: A toolbox for modeling and optimization in MATLAB," in *Proc. IEEE Int. Conf. Robot. Automat.*, 2004, pp. 284–289. [Online]. Available: https://yalmip.github.io/

[39] MOSEK ApS, *The MOSEK Optimization Software*, 2011. [Online]. Available: http://www.mosek.com

[40] SDPT3, Optimization Software, 1999. [Online]. Available: https://github.com/SQLP/SDPT3